Numerical investigation of heat transfer and fluid flow of water through a circular tube induced with divers tape inserts

Taiwo O. Oni [a, *, 1] and Manosh C. Paul [a]

[a] Systems, Power and Energy Research Division, School of Engineering

University of Glasgow, Glasgow G12 8QQ, UK

*Corresponding author. Email: tooni1610@yahoo.com, Tel.: +234(0)803 621 7934

Abstract

An investigation was carried out to analyse numerically heat transfer and flow characteristics of water through a circular tube induced with different twisted tapes. The aim is to know which of the tube designs gives the best performance when compared with a plain tube. Turbulent flow was considered, the walls of the tubes were under uniform wall heat flux, Reynolds number was between 5000 and 20000, and RNG κ-ε model was selected for the simulations. The shape of cuts on the tapes has effects on the performance of the induced tubes. The tube fitted with alternate-axis triangular cut twisted tape has the best performance as its Nusselt number and friction factor are 1.63 – 2.18 and 2.60 – 3.15 times respectively that of the tube fitted with plain twisted tape while its thermal performance factor is 1.35 – 1.43 times that of the tube with plain twisted tape. New correlations were developed for the Nusselt number and friction factors, and reveal that the Nusselt number obtained from the new correlation agrees well with the correlation proposed by Thianpong et al. with a discrepancy of 2.21%. For the friction factor, the discrepancy is 3.01%.

Keywords: Turbulent flow, Heat transfer, Flow characteristics, Numerical simulation

1. Introduction

Thermal energy is utilized in industrial and domestic activities such as in food processing plants, thermal power plants, air conditioning equipment, etc. In all these applications, there is a quest for effective utilization and conservation of thermal energy. The production of these heat exchangers involves huge investments for capital and operation costs [1-3]. In view of the need to reduce the financial resources spent on producing thermal energy, it has become important to devise heat exchanger that is more efficient in performance [4, 5] and also save cost and energy [6, 7]. To achieve this, enhancement of heat transfer becomes applicable and important.

The use of twisted- tape to enhance heat transfer has some benefits that has made its technology a reliable technique. These benefits are its easy installation, low cost and low maintenance [4, 8]. The resistance to

[1] Present address: Mechanical Engineering Department, Faculty of Engineering, Ekiti State University, P.M.B. 5363, Ado-Ekiti, Nigeria; E-mail: tooni1610@yahoo.com, Tel.: +234(0)803 621 7934

heat flow in a heat exchanger is broken by the disturbance introduced to the flow by the twisted-tape and therefore allow more heat to be transferred [3, 9, 10]. The enhancement of heat transfer in a tube fitted with twisted-tape is attributed to the reduction in hydraulic diameter, the secondary motion generated by the twisted tape, and the partitioning and blockage of the tube cross section by the tape [11].

Numerous experimental and numerical investigations have been carried out by various researchers to study the turbulent heat transfer and fluid flow through different tube designs. The investigations which were conducted by Evans and Sarjant [12], Kreith and Margolis[13], Ibragimov et al. [14], and Lopina and Bergles [15] are some of the early works on experimental works on heat transfer enhancement in turbulent flow in tubes induced with twisted tape. An enhancement of up to 50% above that in the plain tube was obtained in all these investigations. Date [16] presented one of the early researches on numerical study of heat transfer enhancement of turbulent flow through tubes induced with twisted tapes and observed that the heat transfer in the induced tube was higher than that in the plain tube.

Kumar and Prasad [17] discovered experimentally that the heat transfer in a solar water heater with a twisted tape can be increased by between 18% and 70% when compared with solar water heater without twisted tape. His report also indicated that the pressure drop can be increased by between 87% and 132% compared to plain solar water heater operating within the same conditions.

Heat transfer enhancement produced by serrated twisted tape was found to be about 1.25 – 1.67 times that in the tube fitted with smooth twisted tape and 2.5 – 4.8 times that in the plain tube. These were the results of experimental study conducted by Chang et al. [18] in their work on turbulent heat transfer and pressure drop in tube fitted with serrated twisted tape.

Eiamsa-ard et al. [19] investigated numerically the effect which the clearance ratio in a tube induced with twisted tape insert has on the Nusselt number and thermal performance factor. The simulation was conducted in the turbulent regime for the Reynolds number ranging from 3000 to 10000. Their findings showed that the tube design with the least clearance provided the best thermal performance.

Murugesan et al. [20] discussed experimentally heat transfer and pressure drop characteristics of turbulent flow with Reynolds number in the range of 2000 to 12000 in a circular tube fitted with trapezoidal-cut twisted tape insert. Their results showed that there was an increase in heat transfer coefficient and friction factor for the tape with trapezoidal-cut. Depending on the twist ratio of the tape, the Nusselt number for the trapezoidal-cut twisted tape was 1.72 to 2.85 times that of the plain tube.

Experimental investigation on heat transfer and friction factor of a double pipe heat exchanger fitted with plain twisted tube and square-cut twisted-tapes for twist ratios 2.0, 4.4 and 6.0 with water as working fluid was conducted by Murusegan et al. [21]. The Nusselt number for the tube induced with square-cut twisted tape of twist ratios 2.0, 4.4 and 6.0 were 1.08, 1.067 and 1.055 respectively times those induced with plain twisted tape. Their friction factors were 1.09, 1.12 and 1.15 respectively times of those for the tube with plain twisted-tape insert.

Cui and Tian [22] investigated experimentally and numerically the heat transfer characteristics and pressure drop in a circular tube induced with edgefold-twisted-tape inserts and with classic spiral-twisted-tape inserts of the same twist ratio. The results indicated that the Nusselt number and friction factor of the tube with

edgefold-twisted-tape inserts were 1.04 to 1.09 times and 1.087 to 1.74 times respectively that of the spiral-twisted-tape inserts.

Through the numerical study carried out by Guo et al. [23], they observed that centre-cleared twisted tape is a promising technique for heat transfer enhancement. Their results revealed that the thermal performance of a tube with centre-cleared twisted tape has an improvement over that of a plain tube, and that the thermal performance of the tube with centre-cleared twisted tape can be enhanced by 7% - 20% compared with those with plain twisted tape.

The numerical analysis of heat and fluid flow through a round tube fitted individually with triple or quadruple twisted tapes of different clearance was investigated by Zhang et al. [24]. The results showed the Nusselt number of the tube with triple twisted tape and quadruple twisted tape has a maximum increase of 171% and 182% respectively over that of the plain tube. In addition, the friction factors of the tube fitted with triple twisted tape and quadruple twisted tape are around 4.06 - 7.02 times that of the plain tube.

In the work of Salman et al. [25], it was discovered numerically that heat transfer in a plain tube can be enhanced by fitting an alternate-axis twisted tape or a plain twisted tape into the plain tube.

Chokphoemphun et al. [26] investigated experimentally the heat transfer and pressure loss characteristics for a turbulent flow by using single, double, triple and quadruple twisted tape inserts in a round tube having a wall subjected to uniform heat flux. The results indicated that the Nusselt number and friction factor for the inserted tubes are in a range of 1.15 - 2.12 times and 1.9 - 4.1 times respectively that for the plain tube.

The effect of tape insert on the heat transfer and the pressure drop through a circular tube at constant wall temperature was studied numerically at Reynolds number up to 600 by Rios-Iribe et al. [27]. It was found that the twisted tape induced a swirling flow, and consequently generated an enhancement in heat transfer.

It is seen in the foregoing paragraphs that several efforts have been made to improve heat transfer by fitting modified twisted tapes inside plain tubes. The modified twisted tapes were made by making cuts on the plain twisted tapes. However, it is evident in the foregoing paragraphs that there has not been a report on either a numerical or an experimental investigation of heat transfer and fluid flow through tubes fitted with twisted tape with emphasis on the cuts on the twisted tapes having different geometrical shapes but equal area. Therefore, this gap is considered in this work.

2. Model geometries

The model geometries are made up of plain tubes induced individually with different designs of twisted tape. The plain tube is shown in Fig. 1(a) and has dimensions of length (L) of 1000mm and internal diameter (D) of 19mm. The different model geometries used, as presented in Fig. 1(a - h), are plain tube (PT), tube with plain twisted tape (TPT), tube with elliptical cut twisted tape (TECT), tube with circular cut twisted tape (TCCT), tube with triangular cut twisted tape (TTCT), tube with alternate-axis elliptical cut twisted tape (TAECT), tube with alternate-axis circular cut twisted tape (TACCT) and tube with alternate-axis triangular cut twisted tape (TATCT). The tubes are sliced so that the tapes inside them can be seen.

The three geometrical shapes chosen as the cuts on the tapes are ellipse, circle, and triangle. Although the cuts have different geometrical shapes, they have the same area (A) of 56.54mm^2. The geometrical

configuration of the plain twisted tape, as depicted in Fig. 1(i), are width (w), thickness (δ) and pitch (y) of 18mm, 1mm and 54mm respectively. The twist ratio (y/w) is 3.

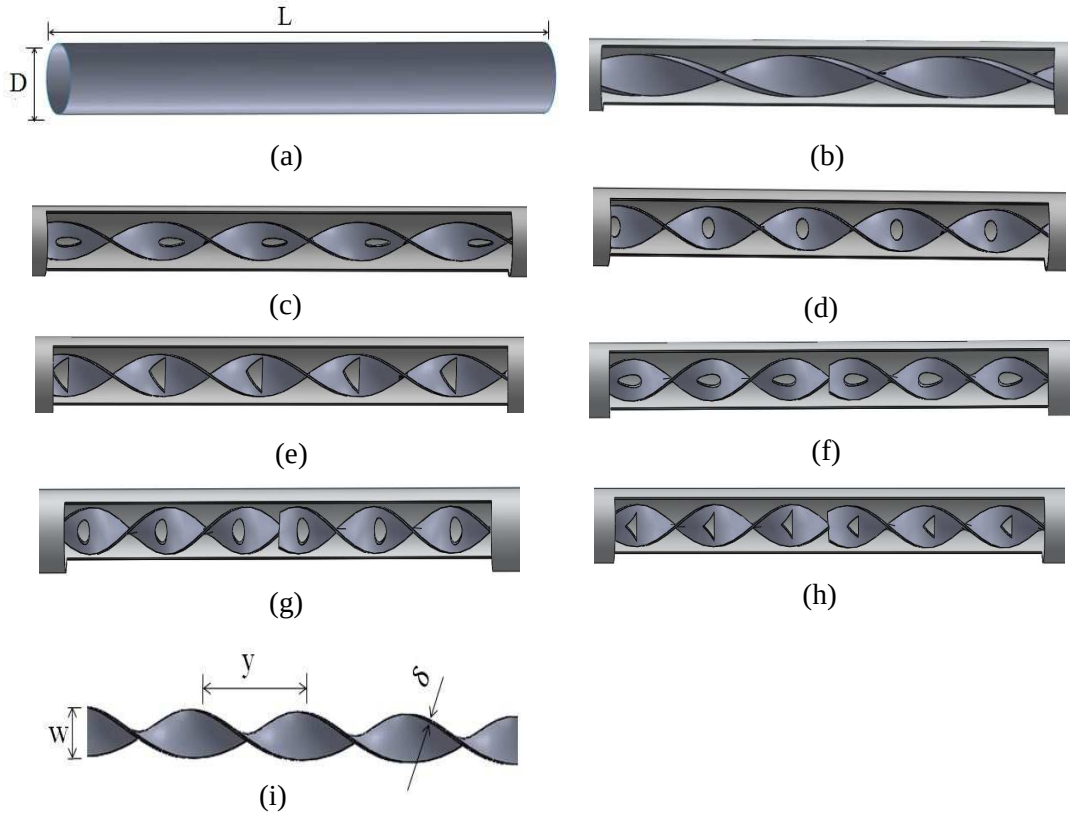

Fig. 1. Model geometries for (a) PT, (b) TPT, (c) TECT, (d) TCCT, (e) TTCT, (f) TAECT, (g) TACCT, (h) TATCT and (i) configuration of plain twisted tape.

3. Governing equations

The working fluid is assumed to be steady and incompressible, and the thermal radiation, chemical reaction and compression work are negligible. The heat transfer is governed by the Navier-Stokes equations of continuity, momentum and energy. Reynolds Averaged Navier-Stokes (RANS) equations are employed to render the Navier-Stokes equations tractable. Mathematical modelling involves numerical solutions of the mass, momentum and energy conservation equations. Based on above assumptions, the governing differential equations are used to describe the heat transfer and fluid flow in the tube. In the following RANS equations, the solution variables represent the time-averaged quantities. The RANS equations [28, 29] are expressed in tensor form as

mass conservation equation:

$$\frac{\partial}{\partial x_i}(u_i) = 0 \tag{1}$$

momentum conservation equation:

$$\rho \frac{Du_i}{Dt} = -\frac{\partial P}{\partial x_i} + \frac{\partial}{\partial x_j}\left[\mu \frac{\partial u_i}{\partial x_j} + \mu\left(\frac{\partial u_i}{\partial x_j} + \frac{\partial u_j}{\partial x_i}\right) - \frac{2}{3} k \delta_{ij}\right] + S_i \tag{2}$$

time-averaged energy equation:

$$\frac{\partial T}{\partial t} + \frac{\partial}{\partial x_j}(u_i T) = \frac{\partial}{\partial x_j}\left(\frac{k_{eff}}{\rho C_p}\frac{\partial T}{\partial x_j} + \frac{\mu_t}{\rho Pr_t}\frac{\partial T}{\partial x_j}\right) \tag{3}$$

The effective thermal conductivity (k_{eff}) is expressed as

$$k_{eff} = k + C_p \frac{\mu_t}{Pr_t} \tag{4}$$

Three different turbulence models were used and their performances were compared. These models are briefly discussed below.

3.1. Standard $\kappa - \varepsilon$ model

The standard $\kappa - \varepsilon$ model [30] is a two-equation turbulence model. The turbulent kinetic energy (κ) is derived from an exact equation by assuming that the effect of the molecular viscosity of the flow is negligible while the turbulence dissipation rate (ε) is obtained by employing physical reasoning [29]. The transport equations [29] for the standard $\kappa - \varepsilon$ model are given as

$$\frac{\partial}{\partial t}(\rho\kappa) + \frac{\partial}{\partial x_i}(\rho\kappa u_i) = \frac{\partial}{\partial x_j}\left[\left(\mu + \frac{\mu_t}{\sigma_\kappa}\right)\frac{\partial \kappa}{\partial x_j}\right] + G_k - \rho\varepsilon \tag{5}$$

$$\frac{\partial}{\partial t}(\rho\varepsilon) + \frac{\partial}{\partial x_i}(\rho\varepsilon u_i) = \frac{\partial}{\partial x_j}\left[\left(\mu + \frac{\mu_t}{\sigma_\varepsilon}\right)\frac{\partial \varepsilon}{\partial x_j}\right] + C_{1\varepsilon}\frac{\varepsilon}{\kappa}G_k - C_{2\varepsilon}\rho\frac{\varepsilon^2}{\kappa} \tag{6}$$

In Eq. (6), the turbulent dynamic viscosity (μ_t) is expressed as

$$\mu_t = \rho C_\mu \frac{\kappa^2}{\varepsilon} \tag{7}$$

and the model constants are $C_{1\varepsilon} = 1.44$, $C_{2\varepsilon} = 1.92$, $C_\mu = 0.09$, $\sigma_\kappa = 1.0$ and $\sigma_\varepsilon = 1.3$ [29].

3.2. RNG $\kappa - \varepsilon$ model

Renormalization Group theory (RNG) $\kappa - \varepsilon$ model [31] is also a two-equation model and it is based on model transport equations for the turbulence kinetic energy (κ) and its dissipation rate (ε) with an additional source term. These equations [29] are

$$\frac{\partial}{\partial t}(\rho\kappa) + \frac{\partial}{\partial x_i}(\rho\kappa u_i) = \frac{\partial}{\partial x_j}\left[\alpha_\kappa \mu_{eff}\frac{\partial \kappa}{\partial x_j}\right] + G_k - \rho\varepsilon \tag{8}$$

$$\frac{\partial}{\partial t}(\rho\varepsilon) + \frac{\partial}{\partial x_i} = \frac{\partial}{\partial x_j}\left[\alpha_\varepsilon \mu_{eff}\frac{\partial \varepsilon}{\partial x_j}\right] + C_{1\varepsilon}\frac{\varepsilon}{\kappa}G_k - C_{2\varepsilon}\rho\frac{\varepsilon^2}{\kappa} - R_\varepsilon \tag{9}$$

The effective dynamic viscosity (μ_{eff}) is expressed as

$$\mu_{eff} = \mu + \mu_t \tag{10}$$

and the model constants are $C_{1\varepsilon} = 1.42$, $C_{2\varepsilon} = 1.68$, $C_\mu = 0.0845$, $\sigma_\kappa = 0.7194$ and $\sigma_\varepsilon = 0.7194$ [29].

3.3. Standard $\kappa - \omega$ model

The standard $\kappa - \omega$ model [32] incorporates modification of low –Reynolds-number effect. It is based on transport equation of turbulence kinetic energy (κ) and specific dissipation rate (ω). Its transport equations [29] as

$$\frac{\partial}{\partial t}(\rho\kappa) + \frac{\partial}{\partial x_i}(\rho\kappa u_i) = \frac{\partial}{\partial x_j}\left[(\mu + \frac{\mu_t}{\sigma_\kappa})\frac{\partial \kappa}{\partial x_j}\right] + G_k - \beta_1\kappa\omega \tag{11}$$

$$\frac{\partial}{\partial t}(\rho\omega) + \frac{\partial}{\partial x_i}(\rho\omega u_i) = \frac{\partial}{\partial x_j}\left[\left(\mu + \frac{\mu_t}{\sigma_\omega}\right)\frac{\partial \omega}{\partial x_j}\right] + G_\omega - \beta_2\omega^2 \tag{12}$$

The turbulent viscosity (μ_t) is written as

$$\mu_t = \frac{\rho\kappa}{\omega} \tag{13}$$

and the model constants are $\beta_1 = \beta_2 = 0.072$.

4. Fluid properties and boundary conditions

The expressions which are provided by Kays and Crawford [33] are used to determine the thermal properties of the working fluid. These properties are density (ρ), specific heat capacity (C_p), thermal conductivity, (k) and viscosity (μ) of 996.6 kg/m^3, 4179 $J/kg.K$, 0.613 $W/m.K$ and 0.000855 $N.s/m^2$ respectively.

The RANS equations and transport equations in §3 above are subject to the following boundary conditions: A uniform heat flux (q), mathematically expressed in Eq. (14), is applied to the surface of tube wall. Also, the wall is subjected to a no-slip condition, represented by Eq. (15). A diameter of 0.019m, a velocity (v), derived by Eq. (16), a temperature of 301K, and an intensity of turbulence (I) as given in Eq. (17) [29] are set at the inlet. The temperature at the fluid-wall interface is expressed in Eq. (18). The axial temperature and velocity gradients at the outlet of the domain are given in Eq. (19). At the outlet of the tube, a zero gauge pressure is specified and other flow quantities are extrapolated from the domain by the solver.

$$-k\left(\frac{\partial T}{\partial x}\right)_{D/2} = q \tag{14}$$

$$(u_i)_{0 \le x \le L} = 0 \tag{15}$$

$$Re = \frac{\rho v D}{\mu} \tag{16}$$

$$I = 0.16Re^{-0.125} \tag{17}$$

$$(T)_{f,\,D/2} = (T)_{w,\,D/2} \tag{18}$$

$$\left(\frac{\partial T}{\partial x}\right)_{x=L} = 0\ ;\ \left(\frac{\partial u}{\partial x}\right)_{x=L} = 0 \tag{19}$$

The turbulence models were activated at a certain time t > 0 after the startup so that the flow took a little time to become fully turbulent. At the inflow boundary, the values of κ, ε and ω were prescribed [29] as

$$\kappa = \frac{3}{2}(uI)^2\ ;\ \ \varepsilon = C_\mu^{3/4}\frac{\kappa^{3/2}}{\ell}\ ;\ \ \omega = \frac{\kappa^{1/2}}{C_\mu^{1/4}\ell} \tag{20}$$

where $\ell = 0.07D$

An enhanced wall treatment is adopted for the simulation of the turbulent flow because it will not significantly reduce the accuracy for wall-function meshes [28, 34].

5. Numerical techniques

The numerical simulation was carried out using Fluent 6.3 [29], a CFD software. The finite volume method was used to discretise the governing partial differential equations. The discretisation was carried out with second order upwind scheme by which the unknown quantities at the cell faces are computed through a Taylor series expansion [35]. As a way of incorporating the effects of pressure into the solution for the momentum equation, the SIMPLE (Semi Implicit Pressure Linked Equations) algorithm [36] was used to couple the calculations of pressure and velocity [28], and Fluent [29] was used to obtain iterative solution of the equations.

6. Grid independence

Grid independence tests were conducted for the domains in order to confirm the accuracy of the numerical solutions. Six grids with different cells were used for each domain as given in Table 1.

Table 1

Grid independence study

Domain	Grid cell					
PT	461178	476554	512420	614904	717388	768630
TPT	913594	944154	1015216	1218259	1421302	1522824
TECT	1122468	1159966	1247298	1496758	1746217	1870947
TCCT	1214178	1254681	1349142	1618970	1888799	2023713
TTCT	1236639	1277931	1374099	1648919	1923739	2061149
TAECT	1486055	1535641	1651206	1981447	2311688	2476809
TACCT	1557545	1609513	1730639	2076767	2422895	2595959
TATCT	1255502	1658638	2515756	3018907	3522058	3773634

Data of temperature and turbulent kinetic energy across the cross-section at the exit of each computational domain for $Re = 20000$ were obtained and depicted in Fig. 2.

The results of the temperature for the grid independence test are shown in Fig. 2. It can be seen that any of the grids with cells 512420, 614904, 717388 and 768630 can be adopted for the PT (Fig. 2(a)) because the difference found among their results are negligible whereas the difference among the results obtained in the

grids with cells 461178, 476554 and 512420 are not negligible. Relying on the pattern of the results obtained for the PT, any of the grids with cells 1015216, 1218259, 1421302 and 1522824 can be adopted for the TPT (Fig. 2(b)); any of the grids with cells 1247298, 1496758, 1746217 and 1870947 can be adopted for the TECT (Fig. 2(c)); any of the grids with cells 1349142, 1618970, 1888799 and 2023713 is appropriate for TCCT (Fig. 2(d)).

Still relying on the pattern of the result obtained above, any of the grids with cells 1374009, 1648919, 1923739 and 2061149 is fit for the TTCT (Fig. 2(e)); any of the grids with cells 1651206, 1981447, 2311688 and 2476809 is suitable for the TAECT (Fig. 2(f)); the TACCT (Fig. 2(g)) can adopt any of the grids with cells 1730639, 2076767, 2422895 and 2595959; any of the grids with cells 2515756, 3018907, 3522058 and 3773634 is suitable for the TATCT (Fig. 2(h)).

Giving consideration to solution precision as well as the time for convergence, the grids with cells 512420, 1015216, 1247298, 1349142, 1374099, 1651206, 1730639 and 2515756 were adopted for the domains PT, TPT, TECT, TCCT, TTCT, TAECT, TACCT and TATCT respectively.

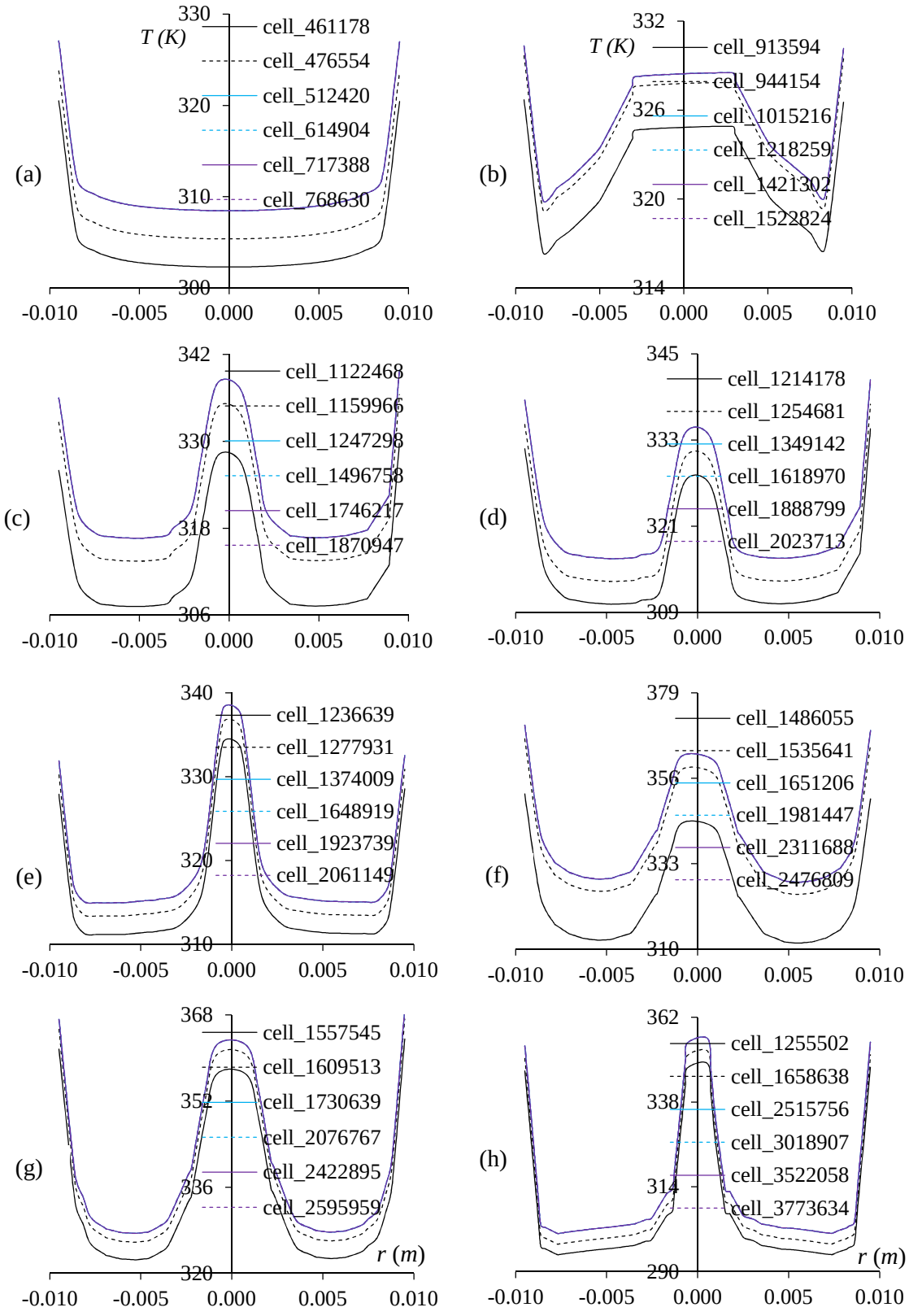

Fig. 2. Temperature across the cross-section at the exit of (a) PT, (b) TPT, (c) TECT, (d) TCCT, (e) TTCT, (f) TAECT, (g) TACCT and (h) TATCT for $Re = 20000$ for different grids.

7. Validation with correlations and experiments

In order to know the models to be selected to perform other numerical simulations, the Nusselt number obtained with the standard $\kappa - \varepsilon$, RNG $\kappa - \varepsilon$ and standard $\kappa - \omega$ turbulence models for the plain tube (PT) and the tube induced with a plain twisted tape insert (TPT) were validated with experimental results and established correlations. The Nusselt number for the PT were validated with the result of Seemawute and Eiamsa-ard experiment [37] and Gnielinski correlation [38]. For the TPT, the validations were carried out with the result of Seemawute and Eiamsa-ard experiment [37], Kidd correlation [39] and Drizius et. al correlation [40].

The validation results of the PT, shown in Fig. 3(a), reveal that the Nusselt number for each of the standard $\kappa - \varepsilon$ and standard $\kappa - \omega$ models is in agreement with the Seemawute and Eiamsa-ard experimental results with a maximum deviation of 8.74%, but the maximum deviation for each of the standard $\kappa - \varepsilon$ and standard $\kappa - \omega$ models is 7.67% when compared with the Gnielinski correlation. For the RNG $\kappa - \varepsilon$ model, the Nusselt number agrees with the experimental results with a maximum deviation of 4.12%, but it agrees with the Gnielinski correlation with a maximum deviation of 6.25%.

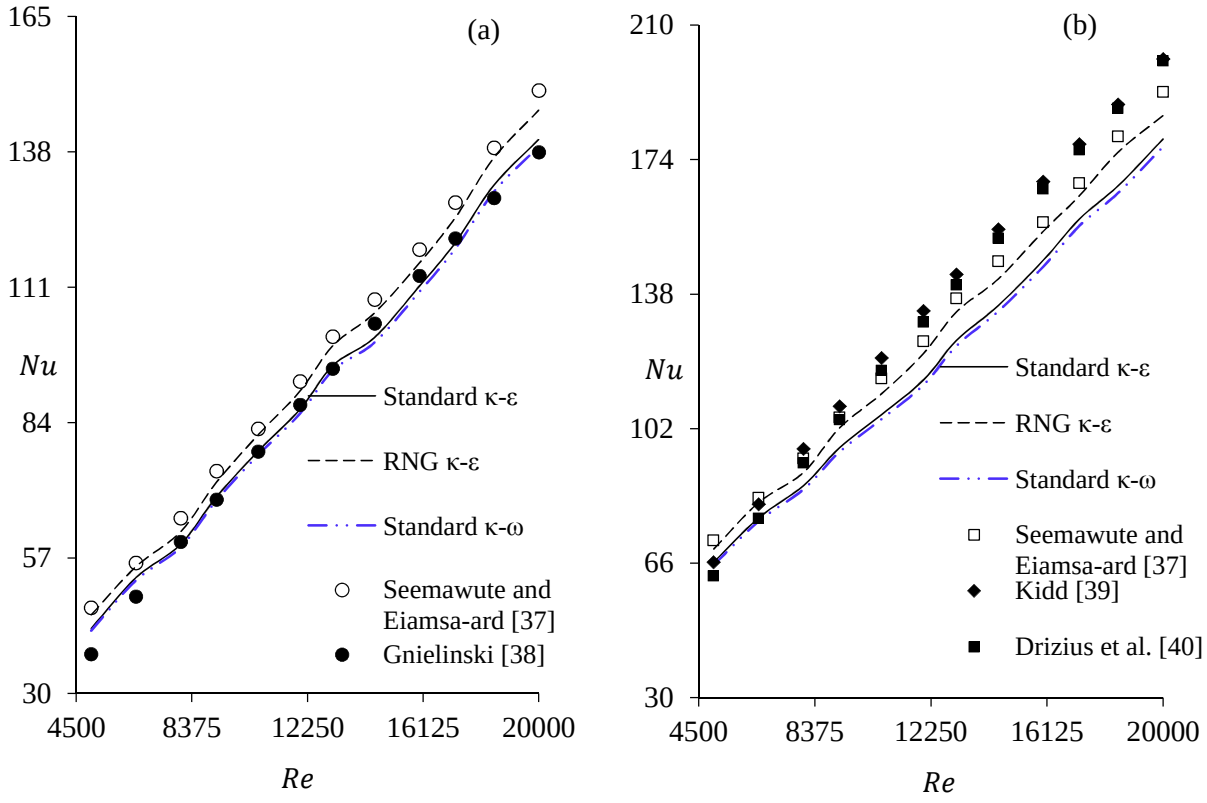

Fig. 3. Validation with standard κ-ε and RNG κ-ε models for (a) PT and (b) TPT.

In the case of the TPT, demonstrated in Fig. 3 (b), the Nusselt number for each of the standard $\kappa - \varepsilon$ and standard $\kappa - \omega$ models agrees with the experimental results with a maximum deviation of 8.33%. Each of the standard $\kappa - \varepsilon$ and standard $\kappa - \omega$ models is in agreement with the Kidd correlation and Drizius et al. correlation is with a maximum deviation of 10.03% and 7.16% respectively. For the RNG κ-ε model, the Nusselt number of the TPT has a maximum deviation of 3.89% when compared with the experimental results

while its agreement with the Kidd correlation and Drizius et al. correlation provides a maximum deviation of 8.54% and 9.11% respectively.

Based on the comparisons presented in the foregoing paragraphs, it is seen that the RNG $\kappa - \varepsilon$ model has an improved performance over the standard $\kappa - \varepsilon$ and standard $\kappa - \omega$ models, and it is more accurate than them. Therefore, the RNG $\kappa - \varepsilon$ model is selected for other numerical simulations in this work.

8. Computational results and discussions

The results with respect to the flow fields, Nusselt number, friction factor and thermal performance are discussed in this section.

8.1. Flow field

Streamlines are drawn in the flow in order to track the path which the particles of the flow follow. The streamlines of the domains at the same axial location 0.866m are shown in Fig. 4. An axial location of 0.866m is considered because this location is near the exit of the domains, and in an induced domain the flow across its cross-sections which have the same type of cut are the same as the flow is approaching the end of the domain [23].

Due to the absence of a twisted-tape in the PT (frame a), the concentration of the streamlines around the wall of the PT (frame a) is weak. With the presence of the twisted tape insert in the TPT (frame b), swirls are

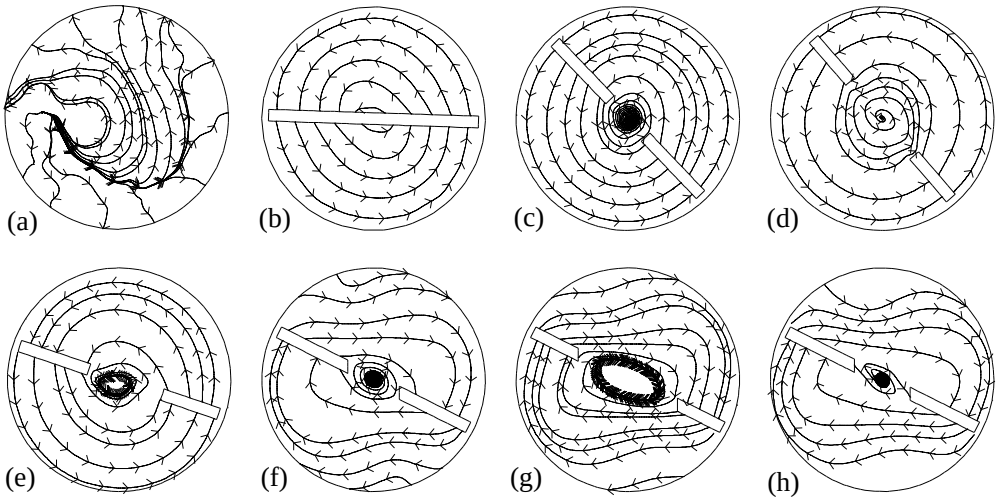

Fig. 4. Streamlines across the domain cross-section at axial location $0.866m$ of (a) PT, (b) TPT, (c) TECT, (d) TCCT, (e) TTCT, (f) TAECT, (g) TACCT and (h) TATCT for $Re = 20000$.

generated and there is a uniform distribution of the streamlines. As a result of additional disturbance and mixing created by the cut in the TECT (frame c), the streamlines have more concentration inside the cut. This pattern is not the same in TCCT (frame d) in which the streamlines inside the cut is widely dispersed due to the periphery of the circular cut having equal distance from the centre of the cut. The streamlines in the TTCT (frame e) concentrate at the centre of the cut due to the edges of the triangular cuts in the TTCT that increase the disturbance more than that in the circular cuts of TCCT (frame d). The cut in the TAECT (frame f) makes the streamlines to concentrate at the centre of the cross-section while the alternate-axis creates additional disturbance to the flow and therefore generates dome-shaped streamlines around the wall

of the domain. The alternate-axis in the TACCT (frame g) also generates dome-shaped streamlines around the wall of the domain, but unlike in the elliptical cut (frame f), the concentration of the cut is further away from the centre of cut. The edge of the triangular cut in the TATCT (frame h) gives a better promotion to the fluid mixing than that of the circular cut (frame g) and therefore its streamline is more concentrated at the centre of the triangular cut (frame h) than that of the circular cut (frame g).

8.2. Temperature contour

The variations in the temperature at randomly-selected locations along the domain are depicted in Fig. 5. In the PT (Fig. 5 (A)), the contours at these locations are approximately the same. This is possibly due to the fact that the flow is developed at these locations. The insertion of plain twisted tape into the plain tube (Fig. 5 (B)) makes the temperature distributions at its locations to improve over that of the PT. This is due to the mixing undergone by the fluid as a result of the twisted tape.

For the TECT (Fig. 5 (C)), the temperature at the axial location $x = 0.673m$ (frame d) is 2.71%, 2.70% and 2.53% higher than those at its axial location $x = 0.5m$ (frame a), $x = 0.516m$ (frame b) and $x = 0.6m$ (frame c) respectively. It is observed that from the location $0.673m$ (frame d) to $0.7m$ (frame e), there is a drop of about 2.01% in the temperature due to absence of cut in the latter. This trend of temperature distribution in the TECT is also applicable to the TCCT (Fig. 5 (D)), and TTCT (Fig. 5 (E)). Due to the presence of cuts at the location 0.516m (frame b), the temperature is 2.11% over those in the upstream (frame a). The presence of the alternate axes (frame c) cause an additional disturbance to the fluid and this results in the generation of thermal energy [41], resulting in 3.17% temperature rise in this region over those of the immediate upstream (frame b). As a result of absence of cut in the downstream region (frame e), its temperature reduces by 1.80% and 2.59% of those in (frame c) and (frame d) respectively.

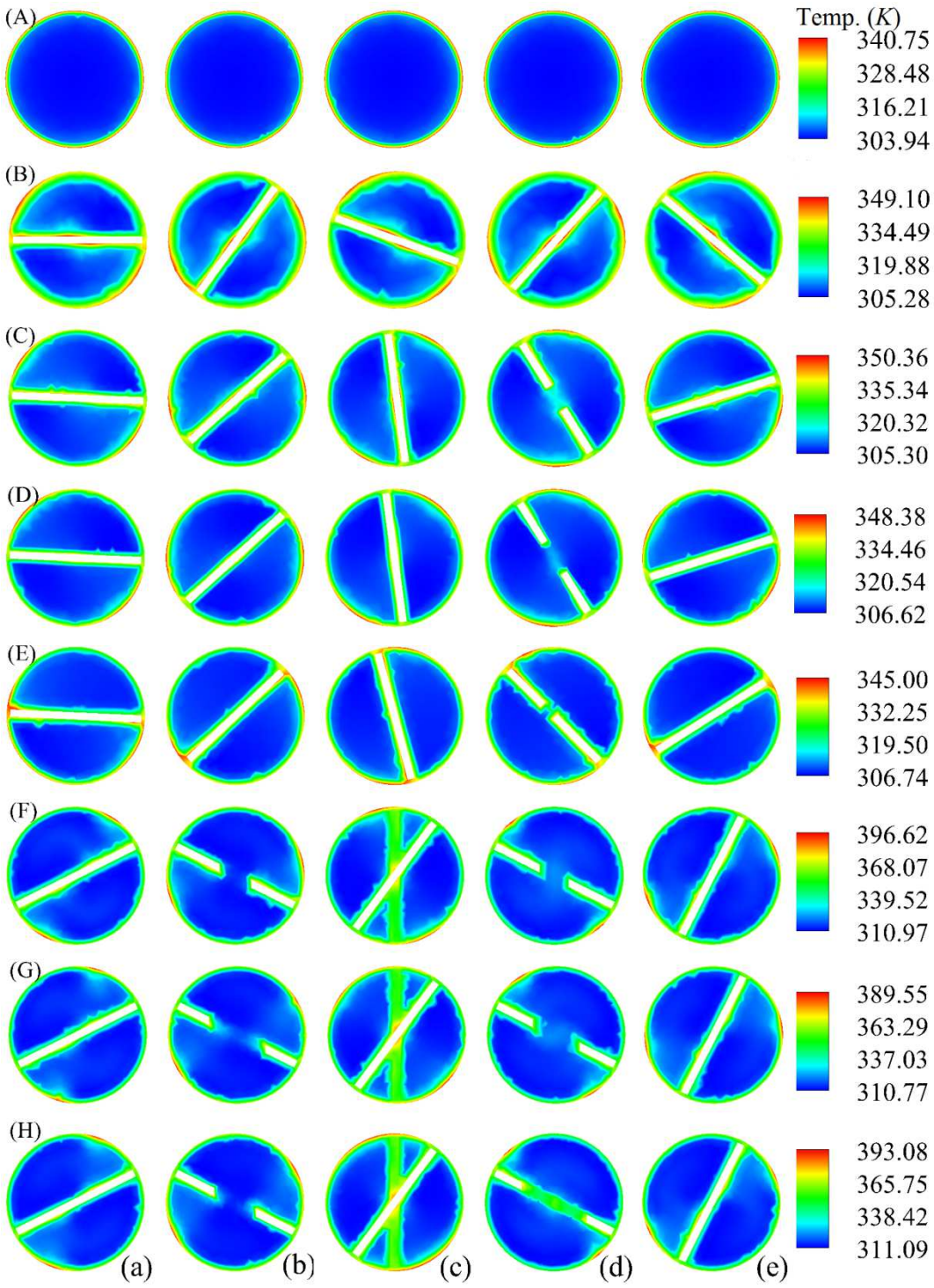

Fig. 5. Contour plots of temperature for PT (A), TPT (B), TECT (C), TCCT (D), TTCT (E), TAECT (F), TACCT (G) and TATCT (H) for $Re = 20000$ at axial location (a) 0.5m, (b) 0.516m, (c) 0.6m, (d) 0.673m and (e) 0.7m.

8.3. Turbulent kinetic energy

The effect of the various domains on the turbulent kinetic energy (TKE) at different locations in the domain is presented in Fig. 6. The maximum TKE in the PT (Fig. 6 (A)) occurs at its wall. The reason for this is that the velocity is minimum at its wall and consequently the TKE at the wall is maximum [42]. When the

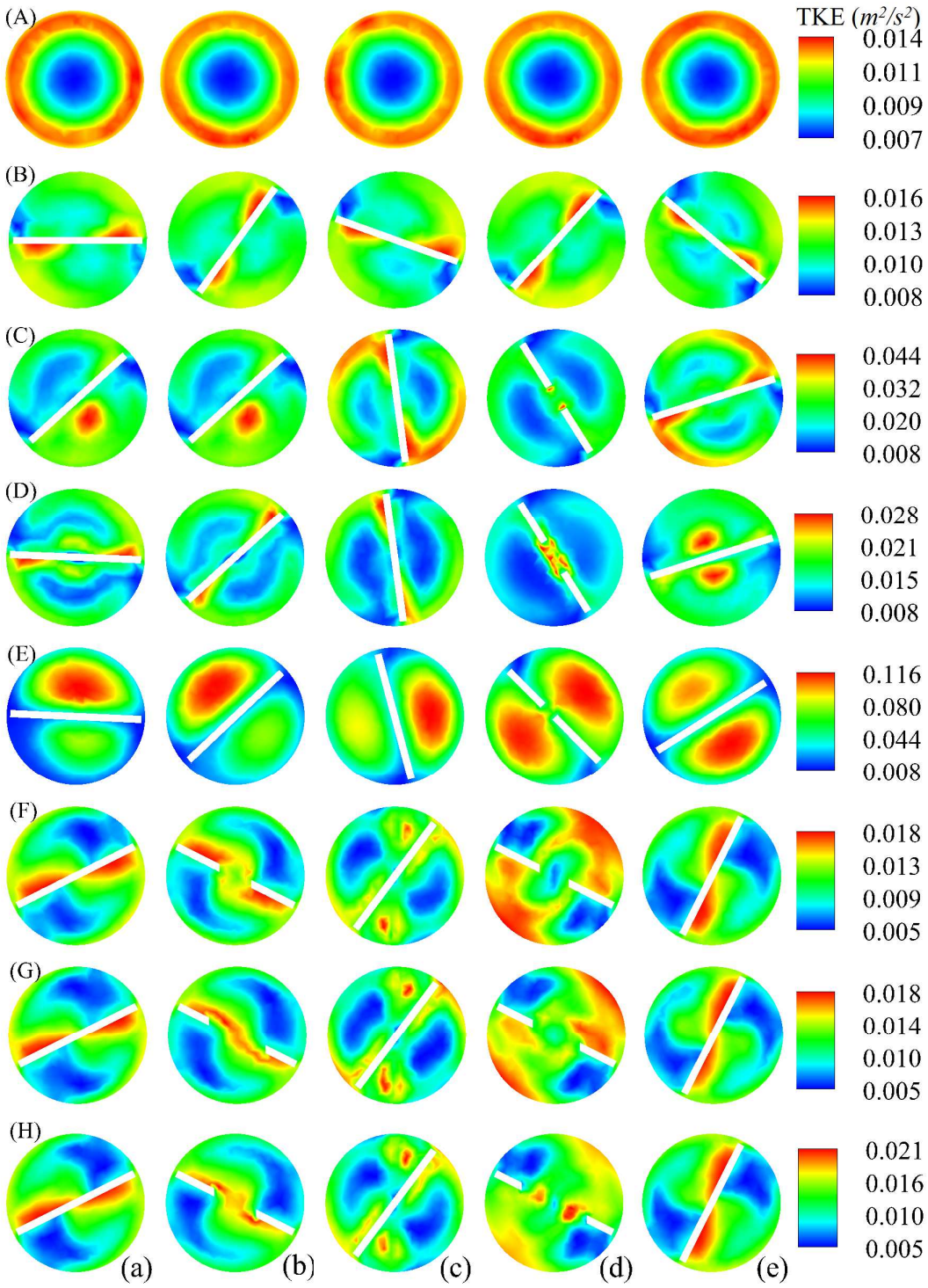

Fig. 6. Contour plots of turbulent kinetic energy (TKE) for PT (A), TPT (B), TECT (C), TCCT (D), TTCT (E), TAECT (F), TACCT (G) and TATCT (H) for $Re = 20000$ at axial location (a) $0.5m$, (b) $0.516m$, (c) $0.6m$, (d) $0.673m$ and (e) $0.7m$.

tube is induced with plain twisted tape, Fig. 6 (B), the swirl flow of the tape makes the TKE to be a maximum near the tape wall and also there is 27.73% increase in the magnitude of the TKE in the TPT compared to that in the PT. The boundary layer which become more turbulent due to the presence of the tape is responsible for this [42]. In the TECT (Fig. 6 (C)), there is a cut on the tape at a location 0.637m (frame d), causing the TKE in this region to be 18.9%, 21.19% and 33.31% respectively higher than those in the

upstream regions (frames a - c). In the further downstream region (frame e), the TKE is 29.28% less than that in the previous region (frame d) in which there are no cuts. The changes in the values of the TKE at the various locations (frame a - e) in the TCCT (Fig. 6 (D)) and TTCT (Fig. 6 (E)) are approximately the same as those in the TECT.

The TKE in TAECT (Fig. 6 (F)), TACCT (Fig. 6 (G)) and TATCT (Fig. 6 (H)) are 11.92%, 13.25% and 17.07% respectively higher than those in TECT (Fig. 6 (C)), TCCT (Fig. 6 (D)) and TTCT (Fig. 6 (E)). This is caused by the alternate axes present in them. In the TAECT (Fig. 6 (F)), the TKE at the location 0.516m (frame b) is 8.68% over those in the upstream (frame a) because of the presence of the cuts at the location 0.516m (frame b). The presence of the alternate axes (frame c) make the TKE to be 10.11% higher than those of the upstream (frame b). The TKE in the frame (c) reduces by 5.24% in the frame (d) and owing to the absence of cut on the tape in the downstream region (frame e) the TKE reduces by 8.66% in this region. In both the TACCT (Fig. 6 (G)) and TATCT (Fig. 6 (H)), the TKE at the location 0.516m (frame b) is 9.38% over those in the upstream (frame a) due to the cuts at the location of 0.516m (frame b). Moreover, the alternate axes at the location 0.6m (frame c) makes the TKE at this location to be 7.2% higher than those at the upstream (frame b). In addition, the TKE at the location 0.6m (frame c) reduces by 4.04% and 6.21% in the frame (d) and frame (e) respectively.

8.4. Assessment of heat transfer

Nusselt number is used to assess the heat transfer and the average Nusselt number (Nu) is given [43] as

$$Nu = \frac{1}{L}\int_0^L h(x)dx.\frac{D}{k} \tag{21}$$

The effect of the different twisted tape on heat transfer is shown in Fig. 7. It is evident in the Figure that as the Reynolds number increases, the Nusselt number also increases. This is due to the turbulent intensity that

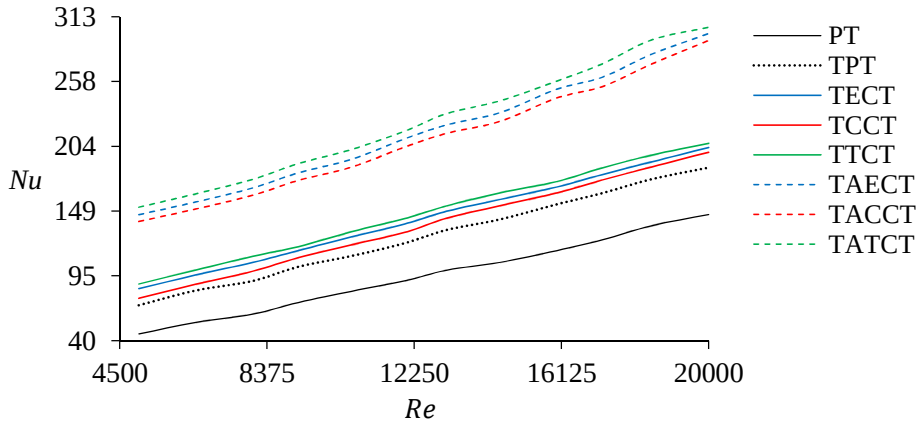

Fig. 7. Effect of different twisted tape on Nusselt number vs. Reynolds number.

increases as the Reynolds number increases, resulting in more destruction of the boundary layer [41]. The Nusselt number of TPT is 1.26 – 1.52 times that of the PT. In addition, the Nusselt number of TECT, TCCT and TTCT are 1.38 – 1.83, 1.35 – 1.65 and 1.41 – 1.91 respectively times that of PT. The Nusselt number of the TAECT, TACCT and TATCT are 2.04 – 3.19, 2.00 – 3.07 and 2.07 – 3.33 respectively times that of PT.

The Nusselt numbers of the induced tubes are higher than those of the PT due to the presence of twisted tape which causes the fluid inside them to swirl with a higher velocity. As a result of better fluid mixing near the wall of the tube caused by the alternate points, their Nusselt numbers are higher than those with twisted tape whose axes do not alternate. As it has been depicted in Fig. 7, the TATCT has the highest Nusselt number.

8.5. Friction factor

Fig. 8 shows the variation of the friction factor with Reynolds number for the different tube designs. The Darcy friction factor (f) is given [43] as

$$f = \frac{2D.\Delta P}{u_m^2.L.\rho} \tag{22}$$

As it has been demonstrated in the Fig. 8, the values of the friction factor are higher at lower Reynolds number. This is because the momentum overcomes the viscous force of the fluid as the Reynolds number increases and in effect lowers the shear between the fluid and the tube wall. Also, due to the absence of swirl flow in the PT it has the least friction factor. Among the induced tubes, the TPT has the lowest friction factor

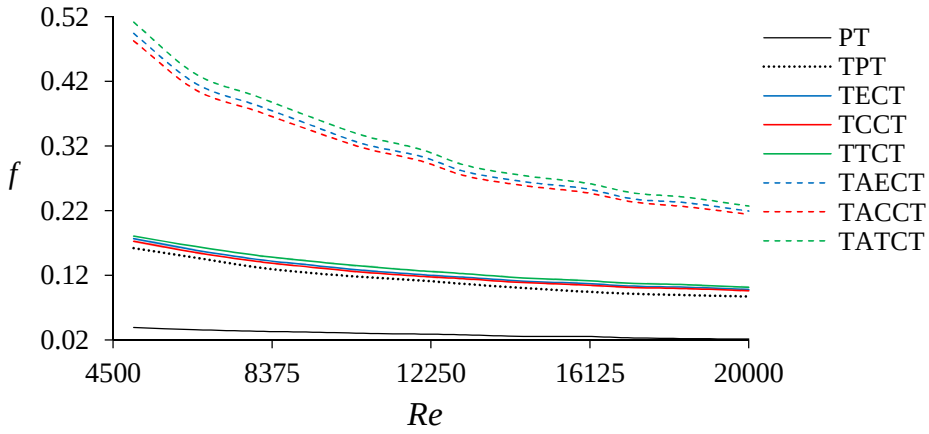

Fig. 8. Effect of different twisted tape on friction factor vs. Reynolds number.

because it has the least blocking effect at the tube wall aside from its least swirling flow. The friction factor of TPT is 4.08 – 4.15 over that of the PT and that of the TCCT is lower compared with the TECT. The friction factor of TECT, TCCT and TTCT are 4.53 – 4.59, 4.42 – 4.50 and 4.62 – 4.76 respectively times that of the PT. The additional dissipation of pressure of the fluid caused by the fluid disturbance due to the presence of cuts on the tapes accounts for the increase in the friction factor of the tapes with cuts over that without cut (TPT). For the TAECT, TACCT and TATCT, their friction factors are 10.29 – 12.66, 10.05 – 12.37 and 10.65 – 13.11 respectively over that of the PT. The more effective fluid disturbance and additional mixing provided by the alternate axes is responsible for this.

8.6. Thermal performance factor

The measure of the possibility of a twisted tape for practical applications in enhancement of heat transfer is referred to as the thermal performance factor (η) of the flow system, and it is mathematically defined [9, 44, 45] as

$$\eta = \frac{Nu}{Nu_p}\left(\frac{f}{f_p}\right)^{-1/3} \tag{23}$$

The variation of the thermal performance factor for the different tube designs is illustrated in Fig. 9. A larger drop in the pressure at higher Reynolds number causes the performance factor to decrease as the Reynolds number increases. The trade-off between the heat transfer and pressure drop yields a promising

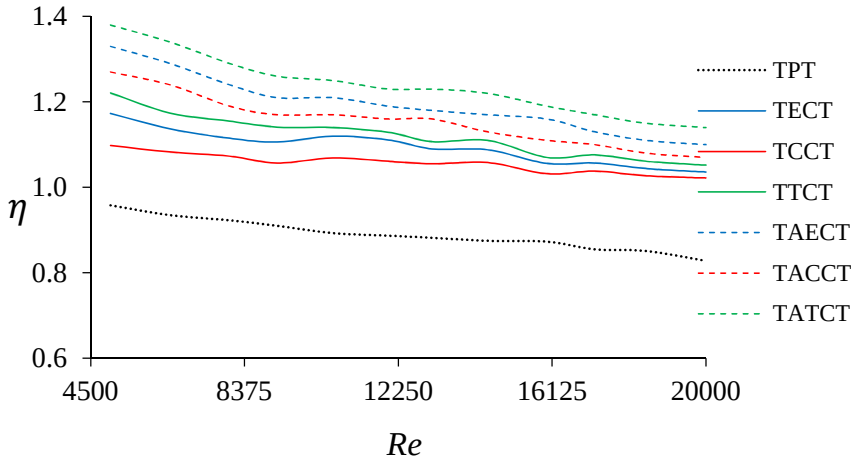

Fig. 9. Effect of different twisted tape on thermal performance factor vs. Reynolds number.

heat transfer enhancement since the thermal performance factors are above unity. The thermal performance factor of TECT, TCCT and TTCT are up to 1.25, 1.23 and 1.27 respectively times that of TPT. For the TAECT, TACCT and TATCT, their thermal performance factors are up to 1.38, 1.32 and 1.43 respectively times that of TPT. For the range of the Reynolds number for which the numerical investigation was conducted, the TATCT has the maximum value of thermal performance factor of 1.43.

9. Correlations for heat transfer and fluid flow

New correlations were developed for the Nusselt number and friction factor of the TAECT, TACCT and TATCT. The correlations for the Nusselt number and friction factor are given in Eq.(24) and Eq. (25) respectively as

$$Nu = 116.961 + Re^{1.323}\, Pr^{-2.938}\left(\frac{p}{w}\right)^{0.296}\left(\frac{y}{w}\right)^{-2.645} \tag{24}$$

$$f = 20.294\, Re^{-0.522}\left(\frac{p}{w}\right)^{0.151}\left(\frac{y/w}{(y/w)-1}\right)^{1.462} \tag{25}$$

Comparisons were made among the numerical results of the present work, the new correlations developed in the present work, and the correlations proposed by Thianpong et al. [46] for the Nusselt number (Fig. 10 (a)) and friction factor (Fig. 10 (b)). The Nusselt number and friction factor obtained from the correlations developed in the present work agree with those of their numerical results with a discrepancy of 2.52% and 4.23% respectively. The Nusselt number obtained from the correlation of Thianpong et al. [46] is in a very

good agreement with those of the correlations developed in the present work with a discrepancy of 2.21%, and for the friction factor it is 3.01%.

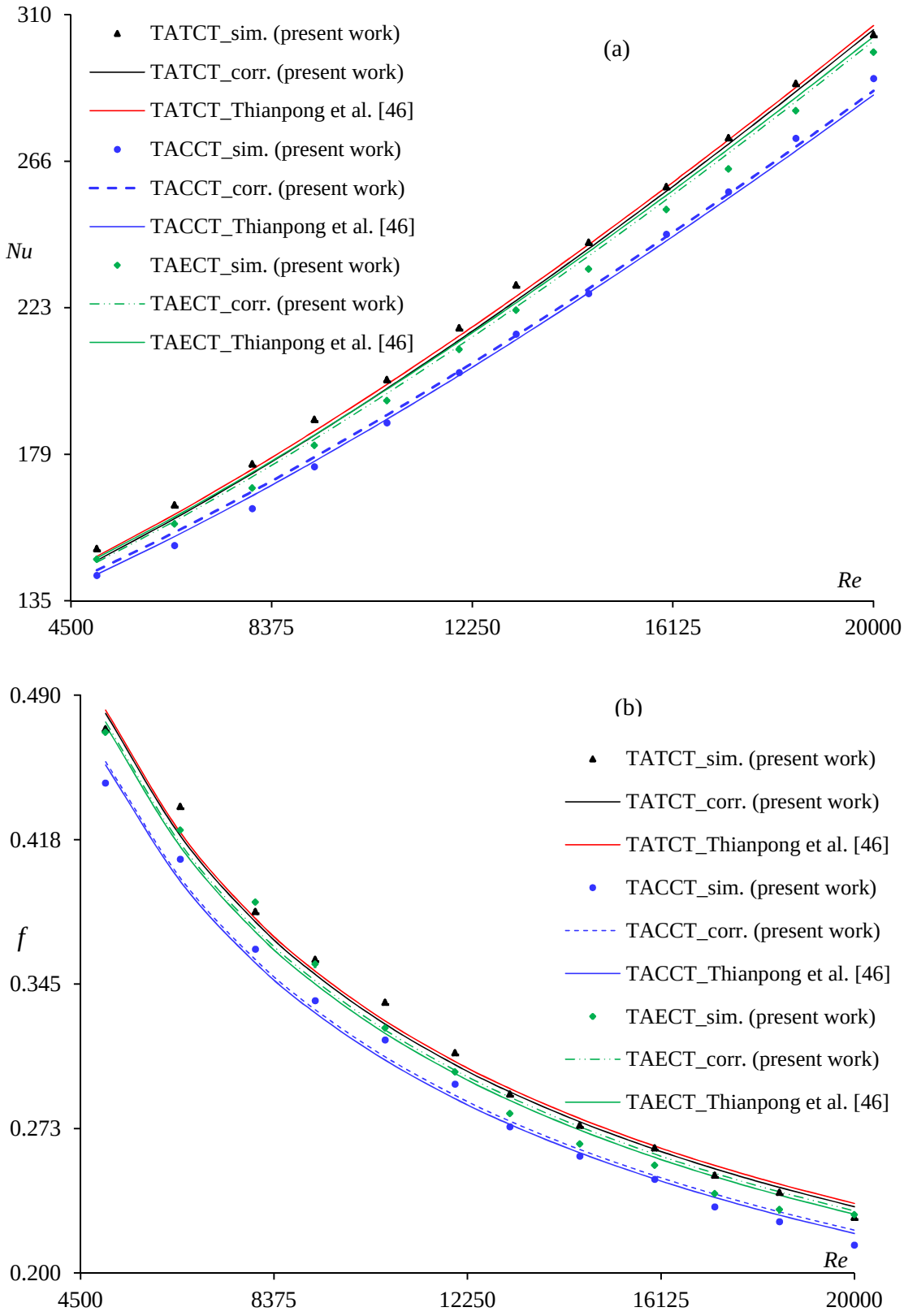

Fig. 10. Comparison between simulated and predicted results for (a) Nusselt number and (b) friction factor.

10. Conclusion

In this study, numerical investigation was conducted on water flow through a circular tube induced with divers twisted tapes in order to investigate its heat transfer and flow characteristics. Reynolds number in the range $5000 \leq Re \leq 20000$ were considered, and RNG $\kappa - \varepsilon$ model was selected for the simulation. The numerical results were validated with experimental results and established correlations, and the results of the validation were found to be in good agreements with one another.

It was discovered that the shape of cuts on the tapes has effects on the performance of the induced tubes, and that the tube with alternate-axis triangular cut twisted tape has the best performance. Its Nusselt number and friction factor are up to 2.18 and 3.15 respectively times that of a tube induced with a plain twisted tape. Its thermal performance factor is up to 1.43 times that of the tube with a plain twisted tape. The Nusselt numbers of the numerical results, the novel correlations of the present work and the established correlation of Thianpong et al. [46] were found to have a very reasonable agreement. This was also the case for the friction factor.

Acknowledgment

Financial support for this research was provided by the Tertiary Education Trust Fund Nigeria and Ekiti State University Ado-Ekiti Nigeria.

References

[1] A. G. Patil, Laminar flow heat transfer and pressure drop characteristics of power-law fluids inside tubes with varying width twisted tape inserts, ASME Trans. J. Heat Transf. 122 (2000) 143-149.

[2] S. K. Saha, A. Dutta, S. K. Dhal, Friction and heat transfer characteristics of laminar swirl flow through a circular tube fitted with regularly spaced twisted-tape elements, Int. J. Heat and Mass Transf. 44 (2001) 4211-4223.

[3] H. J. Lane, P. J. Heggs, Extended surface heat transfer - the dovetail fin, Appl. Therm. Eng. 25 (2005) 2555-2565, http://dx.doi.org/10.1016/j.applthermaleng.2004.11.031.

[4] K. M. Lunsford, Increasing heat exchanger performance, Bryan Research & Engineering Inc., Texas, 1998.

[5] A. E. Bergles, The imperative to enhance heat transfer, in: S. Kakac, A.E. Bergles, F. Mayinger and H. Yuncii, (Eds.), Heat transfer enhancement of heat exchangers, Kluwer, Dordrecht, 1999, pp. 13-29.

[6] D. G. Kumbhar, N. K. Sane, Heat transfer enhancement in a circular tube twisted with swirl flow generator: A review. in: Proc. of the Third Int. Conference on Adv. in Mech. Eng.,Gujarat, India, 2010, pp. 188-192.

[7] L. Wang, B. Sunden, Performance comparison of some tube inserts, Int. Commun. Heat and Mass Transf. 29 (1) (2002) 45-56.

[8] A. Dewan, P. Mahanta, K. S. Raju, P. S. Kumar, Review of passive heat transfer augmentation techniques, Proc. Inst. Mech. Eng. Part A: J. Power and Energy 218 (2004) 509-527, http://dx.doi.org/10.1243/0957650042456953.

[9] Q. Liao, M. D. Xin, Augmentation of convective heat transfer inside tubes with three-dimensional internal extended surfaces and twisted-tape inserts, Chem. Eng. J. 78 (2000) 95-105.

[10] S. Jaisankar, T. K. Radhakrishnan, K. N. Sheeba, S. Suresh, Experimental investigation of heat transfer and friction factor characteristics of thermosyphon solar water heater system fitted with spacer at the trailing edge of left-right twisted tapes, Energy Conversat. Manag. 50 (2009) 2638–2649.

[11] R. M. Manglik, A. E. Bergles, Heat transfer and pressure drop correlations for twisted -tape inserts in isothermal tubes: Part ii - transition and turbulent flows ASME Trans. J. Heat Transf. 115 (1993) 890-896.

[12] S. I. Evans, R. J. Sarjant, Heat transfer and turbulence in gases flowing inside tubes, J. Inst. Fuel 24 (1951) 216-227.

[13] F. Kreith, D. Margolis, Heat transfer and friction in turbulent vortex flow, Appl. Sci. Res. Sect. A 8 (1959) 457-473.

[14] M. H. Ibragimov, E. V. Nomofelov, V. I. Subbotin, Heat transfer and hydraulic resistance with swirl-type motion of liquid in pipes, Teploenenegetika 8 (7) (1961) 57-60.

[15] R. F. Lopina, A. E. Bergles, Heat transfer and pressure drop in tape generated swirl flow of single-phase water, J. Heat Transf. 91 (1969) 434-442.

[16] A. W. Date, Prediction of fully-developed flow in a tube containing a twisted-tape, Int. J. Heat and Mass Transf. 17 (1974) 845-859.

[17] A. Kumar, B. N. Prasad, Investigation of twisted tape inserted solar water heaters – heat transfer, friction factor and thermal performance results, Renew. Energy 19 (3) (2000) 379-398.

[18] S. W. Chang, Y. J. Jan, J. S. Liou, Turbulent heat transfer and pressure drop in tube fitted with serrated twisted tape, Int. J. Therm. Sci. 46 (2007) 506-518, http://dx.doi.org/10.1016/j.ijthermalsci.2006.07.009.

[19] S. Eiamsa-ard, K. Wongcharee, S. Sripattanapipat, 3-D numerical simulation of swirling flow and convective heat transfer in a circular tube induced by means of loose-fit twisted tapes, Int. Commun. Heat and Mass Transf. 36 (2009) 947-955, http://dx.doi.org/10.1016/j.icheatmasstransfer.2009.06.014.

[20] P. Murugesan, K. Mayilsamy, S. Suresh, P. S. S. Srinivansan, Heat transfer and pressure drop characteristics of turbulent flow in a tube fitted with trapezoidal-cut twisted tape insert, Int. J. Acad. Res. 1 (2009) 123-128.

[21] P. Murugesan, K. Mayilsamy, S. Suresh, Turbulent heat transfer and pressure drop in a tube fitted with square-cut twisted tape, Chin. J. Chem. Eng. 18 (4) (2010) 609-617.

[22] Y. Cui, M. Tian, Three-dimensional numerical simulation of thermalhydraulic performance of a circular tube with edgefold-twisted-tape inserts, J. Hydrodyn. 22 (5) (2010) 662-670, http://dx.doi.org/10.1016/S1001-6058(09)60101-3.

[23] J. Guo, A. Fan, X. Zhang, W. Liu, A numerical study on heat transfer and friction factor characteristics of laminar flow in a circular tube fitted with center-cleared twisted-tape, Int. J. Therm. Sci. 50 (2011) 1263-1270, http://dx.doi.org/10.1016/j.ijthermalsci.2011.02.010.

[24] X. Zhang, Z. Liu, W. Liu, Numerical studies on heat transfer and flow characteristics for laminar flow in a tube with multiple regularly spaced twisted tapes, Int. J. Therm. Sci. 58 (2012) 157-167, http://dx.doi.org/10.1016/j.ijthermalsci.2012.02.025.

[25] S. D. Salman, A. A. H. Kadhum, M. S. Takriff, A. B. Mohamad, CFD simulation of heat transfer augmentation in a circular tube fitted with alternative axis twisted tape in laminar flow under a constant heat flux, Heat Transf.-Asian Res. 43 (4) (2014) 384-396, http://dx.doi.org/10.1002/htj.21089.

[26] S. Chokphoemphun, M. Pimsarn, C. Thianpong, P. Promvonge, Thermal performance of tubular heat exchanger with multiple twisted-tape inserts, Chin. J. Chem. Eng. 23 (2015) 755-762, http://dx.doi.org/10.1016/j.cjche.2015.01.003.

[27] E. Y. Rios-Iribe, M. E. Cervantes-Gaxiola, E. Rubio-Castro, J. M. Ponce-Ortega, M. D. Gonzalez-Llanes, C. Reyes-Moreno, O. M. Hernandez-Calderon, Heat transfer analysis of a non-Newtonian fluid flowing through a circular tube with twisted tape inserts, Appl. Therm. Eng. 84 (2015) 225-236, http://dx.doi.org/10.1016/j.applthermaleng.2015.03.052.

[28] H. K. Versteeg, W. Malalasekera, An introduction to computational fluid dynamics- the finite volume method, second ed., Pearson, England, 2007.

[29] Fluent 6.3 user's guide, Lebanon, 2006.

[30] B. E. Launder, D. B. Spaldling, Lectures notes in mathematical models of turbulence, Academic Press, London, 1972.

[31] V. Yakhot, S. A. Orszag, Renormalization group analysis of turbulence I: Basic theory, J. Sci. Comput. 1 (1) (1986) 1-51.

[32] D. C. Wilcox, Turbulence modeling for CFD, DCW Industries Inc, La Canada, California, 1998.

[33] W. M. Kays, M. E. Crawford, Convection heat and mass transfer, second ed., McGrawHill, New York, 1980.

[34] H. Schlichting, Boundary-layer theory, seventh ed., McGraw-Hill, New York, 1979.

[35] C. T. Shaw, Using computational fluid dynamics, Prentice Hall International Ltd., UK, 1992.

[36] S. V. Patankar, D. B. Spalding, A calculation procedure for heat, mass and momentum transfer in three-dimensional parabolic flows, Int. J. Heat and Mass Transf. 15 (1972) 1787-1806.

[37] P. Seemawute, S. Eiamsa-ard, Thermohydraulics of turbulent flow through a round tube by peripherally-cut twisted tape with an alternate axis, Int. Commun. Heat and Mass Transf. 37 (2010) 652-659, http://dx.doi.org/10.1016/j.icheatmasstransfer.2010.03.005.

[38] V. Gnielinski, New equations for heat and mass transfer in turbulent pipe and channel flow, Int. Chem. Eng. 16 (2) (1976) 359-368.

[39] G. J. Kidd, Heat transfer and pressure drop for nitrogen flowing in tubes containing twisted tapes, Am. Inst. Chem. Eng. 15 (1969) 581-585.

[40] M. R. Drizius, R. K. Shkema, A. A. Shlanciauskas, Heat transfer in a twisted stream of water in a tube, Int. Chem. Eng. 20 (1980) 486-489.

[41] K. Wongcharee, S. Eiamsa-ard, Heat transfer enhancement by twisted tapes with alternate-axes rectangular and trapezoidal wings, Chem. Eng. Process. 50 (2011) 211 - 219, http://dx.doi.org/10.1016/j.cep.2010.11.012.

[42] P. R. Lang, F. S. Lombargo, Atmospheric turbulence, meteorological modeling and aerodynamics, Nova Science Publishers, 2010.

[43] F. P. Incropera, D. P. Dewitt, T. L. Bergman, A. S. Lavine, Fundermentals of heat and mass transfer, sixth ed., John Wiley and sons, USA, 2007.

[44] M. A. Akhavan-Behabadi, R. Kumar, A. Mohammadpour, M. Jamali-Asthiani, Effect of twisted tape insert on heat transfer and pressure drop in horizontal evaporators for the flow of R-134a, Int. J. Refrig. 32 (2009) 922-930, http://dx.doi.org/10.1016/j.ijrefrig.2008.11.004.

[45] K. Wongcharee, S. Eiamsa-ard, Friction and heat transfer characteristics of laminar swirl flow through the round tubes inserted with alternate clockwise and counter-clockwise twisted-tapes, Int. Commun. Heat and Mass Transf. 38 (2011) 384-352, http://dx.doi.org/10.1016/j.icheatmasstransfer.2010.12.007.

[46] C. Thianpong, P. Eiamsa-ard, S. Eiamsa-ard, Heat transfer and thermal performance characteristics of heat exchanger tube fitted with perforated twisted-tapes, Heat and Mass Transf. 48 (2012) 881–892, http://dx.doi.org/10.1007/s00231-011-0943-0.

Nomenclature

A	Area (m^2)
$C_{1\varepsilon},\ C_{2\varepsilon}, C_{\mu}$	Model constant
C_p	Specific heat capacity at constant pressure ($J/kg.K$)
c	Clearance between the edge of tape and tube
D	Diameter of tube (m)
f	Friction factor
G_{κ}	Generation of turbulence kinetic energy due to the mean velocity gradients
G_{ω}	Generation of specific dissipation rate
h	Heat transfer coefficient ($W/m^2.K$)
I	Intensity of turbulence
k	Thermal conductivity ($W/m.K$)
L	Length of tube (m)
Nu	Nusselt number
P	Pressure (N/m^2)
p	Perimeter of cut on twisted tape (m)
Pr	Prandtl number
q	Heat flux (W/m^2)
Re	Reynolds number
R_{ε}	Term relating to the mean strain and turbulence quantities
S_i	Source term
t	Time (s)
T	Temperature (K)
u_i, u_j	Time averaged velocity component (m/s)
w	Width of twisted tape (m)
x	Axial coordinate (m)
y	Pitch of twisted tape (m)

Greek symbols

α_{ε}	Inverse Prandtl numbers for ε
α_{κ}	Inverse Prandtl numbers for κ
$\beta_1,\ \beta_2$	Model constant
δ_{ij}	Kronecker delta
δ	Thickness of tape (m)
ε	Dissipation rate of turbulent kinetic energy (m^2/s^3)
η	Thermal performance factor
κ	Turbulent kinetic energy (m^2/s^2)
ℓ	Turbulence length scale (m)
μ	Dynamic viscosity (kg/ms)
ρ	Density (kg/m^3)
σ_{ε}	Prandtl numbers for ε
σ_{κ}	Prandtl numbers for κ
ω	Specific dissipation rate (K^{-1})

Subscripts

b	Bulk
eff	Effective
f	Fluid
i	Inlet
m	Mean
p	Plain tube
t	Turbulent
w	Wall

Nomenclature for equations

Eq. (1) mass conservation equation

Eq. (2) momentum conservation equation

Eq. (3) time-averaged energy equation

Eq. (4) effective thermal conductivity equation

Eq. (5) transport equation for turbulent kinetic energy for standard $\kappa - \varepsilon$ model

Eq. (6) transport equation for turbulence dissipation rate for standard $\kappa - \varepsilon$ model

Eq. (7) turbulent dynamic viscosity equation for standard $\kappa - \varepsilon$ model

Eq. (8) transport equation for turbulent kinetic energy for RNG $\kappa - \varepsilon$ model

Eq. (9) transport equation for turbulence dissipation rate for RNG $\kappa - \varepsilon$ model

Eq. (10) turbulent dynamic viscosity equation for RNG $\kappa - \varepsilon$ model

Eq. (11) transport equation for turbulent kinetic energy for standard $\kappa - \varepsilon$ model

Eq. (12) transport equation for specific dissipation rate for standard $\kappa - \omega$ model

Eq. (13) turbulent dynamic viscosity equation for standard $\kappa - \omega$ model

Eq. (14) equation for heat flux

Eq. (15) equation for velocity at the wall

Eq. (16) equation for Reynolds number

Eq. (17) equation for intensity of turbulence

Eq. (18) temperature at the fluid-wall interface

Eq. (19) axial temperature and velocity gradients at the outlet of the domain

Eq. (20) inflow boundaries for of κ, ε and ω

Eq. (21) equation for average Nusselt number

Eq. (22) equation for Darcy friction factor

Eq. (23) equation for thermal performance factor

Eq. (24) equation for proposed correlation of Nusselt number

Eq. (25) equation for proposed correlation of friction factor